Sensitivity analysis of extreme loads acting on a point-absorbing wave energy converter

Claes Eskilsson, Johannes Palm, Pär Johannesson
and Guilherme Moura Paredes

Abstract—**There are many uncertainties associated with the estimation of extreme loads acting on a wave energy converter (WEC). In this study we perform a sensitivity analysis of extreme loads acting on the Uppsala University (UU) WEC concept. The UU WEC consists of a bottom-mounted linear generator that is connected to a surface buoy with a taut mooring line. The maximum stroke length of the linear generator is enforced by end-stop springs. Initially, a Variation Mode and Effect Analysis (VMEA) was carried out in order to identify the largest input uncertainties. The system was then modelled in the time-domain solver WEC-SIM coupled to the dynamic mooring solver Moody. A sensitivity analysis was made by generating a surrogate model based on polynomial chaos expansions, which rapidly evaluates the maximum loads on the mooring line and the end-stops. The sensitivities are ranked using the Sobol index method. We investigated two sea states using equivalent regular waves (ERW) and irregular wave (IRW) trains. We found that the ERW approach significantly underestimate the maximum loads. Interestingly, the ERW predicted wave height and period as the most important parameters for the maximum mooring tension, whereas the tension in IRW was most sensitive to the drag coefficient of the surface buoy. The end-stop loads were most sensitive to the PTO damping coefficient.**

Index Terms—**end-stops, extreme waves, generalized polynomial chaos, mooring dynamics, sensitivity analysis, variation mode effect analysis, wave energy converter.**

I. Introduction

SURVIVABILITY remains a major challenge of the wave energy sector. During sea-trials the sector has experienced repeated failures connected to storms and harsh seas. Often the failures have occurred in the station-keeping sub-system, e.g. the Oceanlinx [1] and CETO 4 [2] devices. Another relevant example for the present study is the breaking of the mooring wires of the Seabased WECs at the farm outside Lysekil, Sweden, during the Storm Urd around Christmas time in 2016 [3] (the Storm Urd allegedly gave rise to waves up to 12 m high, to be compared to the maximum wave height of 14.12 m ever recorded in the Skagerrak [4]).

As survival design is closely linked to capital expenditure (CAPEX) there is an interest in looking into the uncertainty of the predicted maximum loads; and there are many uncertainties associated with the estimation of extreme loads acting on a wave energy converter (WEC). At a first glance the major uncertainty is often assumed to arise from the choice of design case, being closely related to the estimation of the Nth-year contour line. Here there are different approaches. Popular choices include the 'all sea-states' approach, the inverse first-order method and the one-dimensional design load selection approach. These methods will yield different results using the same input data, see e.g. the discussion in [5]. However, the present paper does not go into detail with regard to estimation of design cases. We focus on the combined uncertainties from several input variables, which apart from the environmental loads include the properties of the subsystems of the WEC itself (the surface buoy, the mooring line and the linear generator). In order to assess the sensitivity of the system and build probability density functions (PDF), we need to propagate the random input variables forward through the nonlinear system.

A straightforward approach for this is to run Monte Carlo (MC) simulations of the entire system. However, even for models based on linear potential flow MC simulations quickly become prohibitively expensive. Thus, we need to build a surrogate model that is cheap to evaluate. In this paper we will employ surrogate models based on generalized Polynomial Chaos (gPC) [8], [9]. We note that there are several other types of surrogate models available, e.g. Kriging [6] and artificial neural networks [7]. A main reason of gPC popularity is due to the non-intrusive approach, i.e. it works as a wrapper around the deterministic model and no changes are required within the deterministic model. The gPC methodology has been used in the marine sector for estimating wave propagation over uncertain bathymetry [10]; for uncertainty quantification of mooring loads [11], [12]; and for extreme loads on wave energy converters [13]. Please note that [13] uses a gPC approach to create a surrogate model for significant wave height and peak period to

Manuscript received December 30th, 2021, published 10 June 2022.

This work was supported by the Swedish Energy Agency under project number 47264-1.
C. Eskilsson is with the Renewable Energy Unit, RISE – Research Institutes of Sweden, Box 857, SE-501 15 Borås, Sweden (e-mail: claes.eskilsson@ri.se); and the Department of the Built Environment, Aalborg University, Thomas Manns Vej 23, DK-9220 Aalborg Ø, Denmark (e-mail: claese@build.aau.dk).

J. Palm is with Sigma Energy & Marine AB, Ekelundsgatan 1-3, SE-411 18 Gothenburg, Sweden (e-mail: johannes.palm@sigma.se).

P. Johannesson is with the Applied Mechanics Unit, RISE – Research Institutes of Sweden, Box 857, SE-501 15 Borås, Sweden (e-mail: par.johannesson@ri.se).

G. Moura Paredes is with Development and Research in Environment, Applied Management and Space, Universidade Lusófona do Porto, Rua Augusto Rosa, no 24, 4000-098, Porto, Portugal (e-mail: guilherme.paredes@ulp.pt).
Digital Object Identifier: https://doi.org/10.36688/imej.5.91-101

efficiently evaluate the loads using the 'all sea-states' approach. The present study aims to also account for the uncertainties from the WEC system.

Even if the gPC surrogate model is cheap to evaluate, there is of course a computational cost associated with constructing the gPC model. This cost grows rapidly with the number of the input random variables d; the so-called curse of dimensionality. The cost to construct the gPC model using all possible variables is thus prohibitive. In order to find the supposedly most influential variables this study employs a Variation Mode and Effect Analysis (VMEA) [14], [15]. VMEA is a probabilistic method that studies the variation and uncertainty around a nominal design. The VMEA approach represents a first order, second moment reliability method. "First order" is due to the fact that the influence of each term is approximated by one single linear term, and "second moment" is that the probabilistic influence is approximated by second moment statistics, variances and covariances.

A. Paper contribution

In this paper we present a sensitivity analysis of the resulting extreme loads acting on the WEC developed by Uppsala University (UU). The UU WEC is a point-absorber with a shallow draft surface buoy connected with a wire to a direct-drive linear generator standing on the sea-floor (the design is similar to the WEC developed by Seabased), see Fig. 1 [16]. The most influential parameters are found by performing an initial VMEA analysis of the system. The identified parameters are then treated as random inputs and gPC surrogate models are created using a non-intrusive collocation method around the deterministic WEC model made in the linear potential flow solver WEC-SIM [17] and the mooring solver Moody [18]. Both the VMEA and gPC methodologies have been independently applied to wave energy cases before [13], [19], but to the authors best knowledge this is the first time they are used together within the maritime sector.

II. Building surrogate models using generalized Polynomial Chaos

Let $f(\mathbf{x}, Z)$, represent a model where $\mathbf{x}$ is the vector of deterministic input variables and $Z : \Omega \to \mathbb{R}$ is a random variable in the sample space of possible outcomes Ω. Using the property that a continuous function in L_2 with bounded variation can be expressed as an infinite series, gPC provides a polynomial expansion surrogate model to $f(\mathbf{x}, Z)$ [9]:

$$f_{gPC}(\mathbf{x}, Z) \approx \sum_{k=0}^{p} \hat{f}_k(\mathbf{x})\phi_k(Z)\,, \tag{1}$$

where the infinite sum has been truncated at the specified polynomial degree p. Here $\hat{f}_k(\mathbf{x})$ are the polynomial coefficients and $\{\phi_k(Z)\}_{k=0}^{p}$ is the set of polynomial basis functions. For optimal convergence of $f_{gPC}(\mathbf{x}, Z)$ to the results of the original model $f(\mathbf{x}, Z)$, the basis functions should be selected based on the probability distribution of Z according to the Wiener-Askey scheme [8].

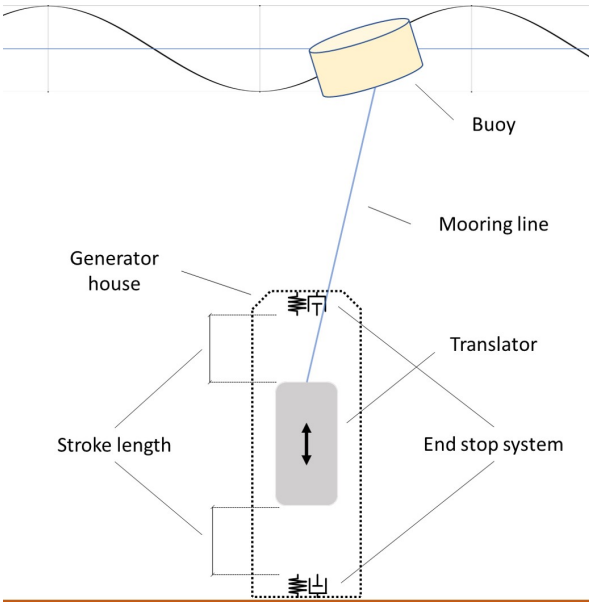

Fig. 1. Outline of the modelled UU WEC system. Please note that the figure is not according to scale.

For problems with several random input variables, $\mathbf{Z} : \Omega \to \mathbb{R}^d$ denotes the d-dimensional vector of random variables and (1) is replaced by a tensor product of polynomials corresponding to each random variable

$$\begin{aligned} f_{gPC}(\mathbf{x}, \mathbf{Z}) &\approx \sum_{|\mathbf{k}|=0}^{p} \hat{f}_{\mathbf{k}}(\mathbf{x})\Phi_{\mathbf{k}}(\mathbf{Z}) \\ &= \sum_{|\mathbf{k}|=0}^{p} \hat{f}_{\mathbf{k}}(\mathbf{x})\phi_{k_1}(Z_1)\phi_{k_2}(Z_2)...\phi_{k_d}(Z_d)\,, \end{aligned} \tag{2}$$

where $\mathbf{k}$ is a multi-index such that $\mathbf{k} = (k_1, k_2, ..., k_d)$ and $|\mathbf{k}| = k_1 + k_2 + ... + k_d$, and $\phi_{k_i}(Z_i)$ is the polynomial basis function of the variable Z_i of degree k_i.

A. Stochastic collocation method

To build the gPC surrogate model we use the stochastic collocation method [9]. This is a non-intrusive method, so we only need to post-process the results of simulations using the deterministic model at pre-selected values $\mathbf{z}^{(j)}$ of the uncertain input $\mathbf{Z}$. The points $\mathbf{z}^{(j)}$ where $f(\mathbf{x}, \mathbf{Z})$ is to be evaluated depend on the method chosen to determine the coefficients $\hat{f}_{\mathbf{k}}$. These points are typically chosen at the corresponding quadrature points when $d < 4$, whereas latin hyper cube (LHC) sampling is used for larger d .

B. Sensitivity analysis from gPC

An important feature of the gPC method is that the polynomial coefficients $\hat{f}_{\mathbf{k}}$ encode information about the moments of the probability distributions of the results. Thus, sensitivity analysis is the integral of the gPC method. In Sobol's method for sensitivity analysis [20], a function $f(\mathbf{x}, \mathbf{Z})$ with d random variables is

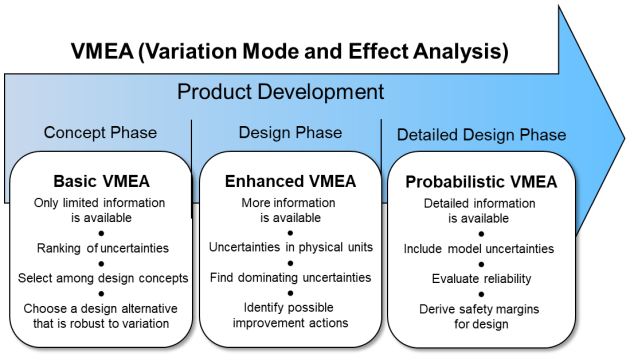

Fig. 2. VMEA in different design stages. From [19].

decomposed in a series summation of functions of increasing order in the variables z_i:

$$f(\mathbf{x},\mathbf{Z}) = f_0 + \sum_i f_i(\mathbf{x},Z_i) + \sum_{i<j} f_{ij}(\mathbf{x},Z_i,Z_j) + \ldots + f_{1\ldots d}(\mathbf{x},Z_1\ldots Z_d). \quad (3)$$

The variance $\mathrm{Var}[f(\mathbf{x},\mathbf{Z})]$ of $f(\mathbf{x},\mathbf{Z})$ is obtained by summing the variance of each term of (3). The variance of each term in (3) can be obtained from the coefficients $\hat{f}_{\mathbf{k}}$ of the gPC model [21]. The sensitivity index describing the contribution of each term to the total variance, $S_{i_1,\ldots,i_d}$, is obtained by the ratio between the variance of that term and the total variance:

$$S_{i_1,\ldots,i_d} = \frac{\mathrm{Var}[f(\mathbf{x},Z_{i_1,\ldots,i_N})]}{\mathrm{Var}[f(\mathbf{x},\mathbf{Z})]} \quad (4)$$

and the total sensitivity index S_i^T for variable Z_i, describing the fraction of the variance caused by variable Z_i at all orders of interaction, is [21]

$$S_i^T = \sum S_{i_1,\ldots,i_d} \quad (5)$$

III. Variation Mode and Effect Analysis

VMEA comes in three flavors associated with different stages of the product development process, see Fig. 2. The first phase is the basic VMEA where standard deviations and sensitivity coefficients are replaced by scores, i.e. relative numerical engineering judgements about uncertainty and sensitivity, respectively. The basic VMEA is used in the early design stage when little is known about variations and be built up from a cooperative brain storm session. It gives a qualitative picture of uncertainty distribution between different sources and be used for prioritisation for further studies.

A refinement of the basic VMEA may be done by quantifying uncertainties by judging their standard deviations by means of standard rules and judge sensitivities by fundamental physical knowledge. This analysis is called an Enhanced VMEA and can be used for a preliminary assessment of a safety factor needed for taking the studied uncertainties into account.

A further refinement, called the probabilistic VMEA, is developed by getting more information about the most critical uncertainty sources. Standard deviations are obtained by more detailed studies of empirical

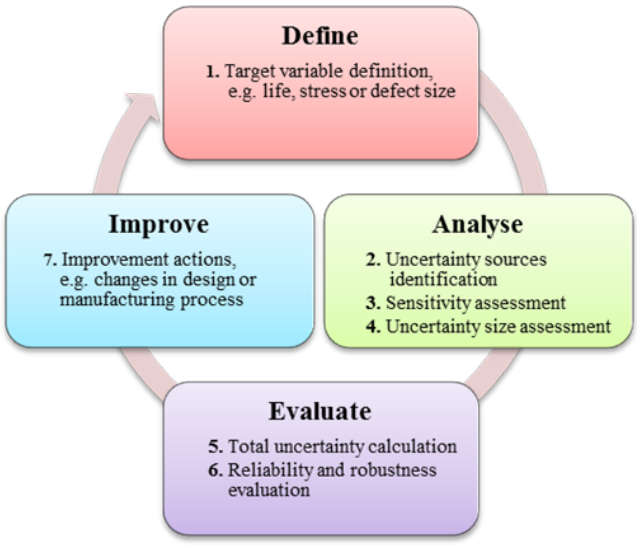

Fig. 3. VMEA in the design and improvement cycle. From [19].

results. Sensitivity coefficients are found from numerical sensitivity studies or differentiation of physical/mathematical models. The result of such an analysis give an estimate of the resulting total uncertainty and a corresponding statistical safety factor.

The general procedure for making a VMEA is common for all development phases. The work process can be split into four activities "Define-Analyse-Evaluate-Improve", as illustrated in Fig. 3, and can be described by the seven steps listed in Fig. 3.

A. Mathematical principles of VMEA

The method is based on characterising each uncertainty source by a statistical standard deviation and calculating its sensitivity with respect to the target variable, such as fatigue life, maximum stress etc. The VMEA method combines these into the total prediction uncertainty, denoted τ, which is obtained by the root sum of squares (RSS) of the uncertainties in (6).

$$\tau = \sqrt{\sum_{i=1}^{n} \tau_i^2} = \sqrt{\sum_{i=1}^{n} c_i^2 \sigma_i^2}\,, \quad (6)$$

where τ_i is the resulting uncertainty from source i. τ_i is calculated as the product of the sensitivity coefficient c_i and the uncertainty σ_i of source i. The total number of uncertainty sources is n. Note that VMEA is a so-called second-moment method since it uses only the standard deviation to characterise the distribution of the uncertainty sources.

B. Evaluation of reliability and uncertainties

As mentioned in the introduction, VMEA is a first order, second moment reliability method that studies the variation and uncertainty around a nominal design. Let us denote a response function as

$$y = f(x_1,\, x_2,\, \ldots,\, x_p)\,, \quad (7)$$

where y is the response and the x_i's are the input parameters. The standard deviation, being the square root

of the variance, is found using the *Gauss' approximation formula*

$$\begin{aligned}\mathrm{Var}[Y] &= \mathrm{Var}[f(X_1,\, X_2,\, \ldots,\, X_p)] \\ &\approx \sum_{i=1}^{n} c_i^2 \mathrm{Var}[x_i] + \text{Covariances}\,. \end{aligned} \tag{8}$$

This formula gives the variance of the target function f as the sum of variance contributions from different influencing random variables X_i, each described by its own variance together with its influence by means of its sensitivity coefficient c_i. The sensitivity coefficients are defined as

$$c_i = \frac{\partial y}{\partial x_i}\,(x_{1,r},\, x_{2,r},\, \ldots,\, x_{p,r}) \tag{9}$$

evaluated at a reference point $(x_{1,r},\, x_{2,r},\, \ldots,\, x_{p,r})$. Formally, the sensitivity coefficient c_i is the partial derivative of the target function f with respect to x_i, but it is often best approximated by a difference quotient. Covariances between the influencing variables also contribute, however they can usually be neglected or avoided by re-formulating the model.

IV. Numerical modelling

A. Hydrodynamic model

The dynamics of the WEC is modelled using the linear potential flow assumption. In time domain we use Cummins' equation [22] to describe the buoy motion:

$$\begin{aligned}&(\mathbf{M} + \mathbf{A}_\infty)\,\ddot{\mathbf{X}}\,(t) + \int_{-\infty}^{t} \mathbf{K}\,(t-\tau)\,\dot{\mathbf{X}}\,(t)\,\mathrm{d}\,\tau \\ &+ \mathbf{C}\mathbf{X}\,(t) = \mathbf{f}_{\mathrm{exc}}\,(t) + \mathbf{f}_{\mathrm{drag}}\,(t) + \mathbf{f}_{\mathrm{moor}}\,(t)\ , \end{aligned} \tag{10}$$

with $\mathbf{M}$ being the generalized mass matrix of the floating body, $\mathbf{A}_\infty$ the added mass matrix at infinite frequency, $\mathbf{K}$ the radiation impulse response function, $\mathbf{C}$ the hydrostatic stiffness matrix, and $\mathbf{X}$, $\dot{\mathbf{X}}$, and $\ddot{\mathbf{X}}$, respectively, the displacement, velocity, and acceleration vectors. The external forces include the wave excitation forces, $\mathbf{f}_{\mathrm{exc}}$, the quadratic drag forces, $\mathbf{f}_{\mathrm{drag}}$, and the mooring forces, $\mathbf{f}_{\mathrm{moor}}$. The hydrodynamic coefficients are computed using the open-source boundary element method (BEM) code Nemoh [23]. Please note that (10) is used for the surface buoy, and the interaction with the bottom-mounted generator and the PTO is through the mooring force $\mathbf{f}_{\mathrm{moor}}$.

The code used to solve Cummins' equation, or the dynamics of the floating structure, is the time-domain multi-body dynamics model WEC-Sim developed by NREL and Sandia [17]. WEC-Sim supports weakly nonlinear simulations by means of the nonlinear Froude-Krylov approach, in which the wave excitation force is estimated using the instantaneous wetted surface. This feature is applied in the simulations.

B. Mooring

We use here the mooring dynamics solver Moody. Moody is based on a high-order discontinuous Galerkin method [18], [24], [25] and the model supports internal rigid bodies used to model submerged buoys and clump weights [26]. This feature has been extended to model the linear generator PTO, see [27]. Moody can be coupled to external hydrodynamic solvers, and the coupling to WEC-SIM used in this work was validated in [28].

C. PTO and end-stops

The dynamics of the direct-driven linear generator including the end-stops are implemented within Moody. The translator is simply treated as a single-degree-of-freedom rigid body subjected to Newton's second law of motion. The generator PTO force is

$$\mathbf{f}_{\mathrm{PTO}} = -C_{\mathrm{PTO}}\dot{z}_t\,, \tag{11}$$

where C_{PTO} is the linear damping coefficient of the PTO and $\dot{z}_t$ is the translator velocity. The upper and lower end-stops are activated if the translator exceed the upper or lower stroke lengths. The end-stops are modelled as a two-stage spring system with the main spring stiffness denoted (K_{es}). Please see [27] for details of the implementation.

V. Case study

A. The Uppsala University WEC

In this work we consider the wave energy converter developed at Uppsala University [16], [29]. A cylindrical buoy is moored with a steel wire rope, which is connected to the translator of a bottom-mounted, vertical linear generator. Fig. 1 schematically describes the WEC system and the relevant subsystem terminology. In addition, the translator and its end-stop system are collectively labelled the Generator.

TABLE I
System specific settings of the baseline UU WEC case.

Buoy		**Mooring line**		**Generator**	
Mass, m_b (kg)	5736	Density, ρ_c (kg/m^3)	5204	Mass, m_t (kg)	6240
Pitch inertia, I_{yy} (kgm^2)	6293	Diameter, D_c (m)	0.04	Stroke length, a_t (m)	1.2
Radius, $0.5D_b$ (m)	1.7	Normal drag coeff., C_{Dn} (-)	1	Damping, C_{PTO} (kNs/m)	59
Height, h_b (m)	2.12	Tang. drag coeff., C_{Dt} (-)	0.1	End stop stiffness, K_{es} (kN/m)	776
Draft (m)	1.3	Young's modulus, E_c (GPa)	15.54	End stop length, L_{es} (m)	0.6
Center of gravity, $z_b^{(g)}$ (m)	-0.25	Material damping, ξ_c (kNs)	1.715	Translator length, L_t (m)	1.8
Heave/surge drag coefficient, $C_D^{(b)}$	1.2	Length, L_c (m)	64.90	Center of gravity, $z_t^{(g)}$	-67.3,
Mooring point, $z_b^{(m)}$ (m)	-1.3			Mooring point, $z_t^{(m)}$ (m)	-66.4

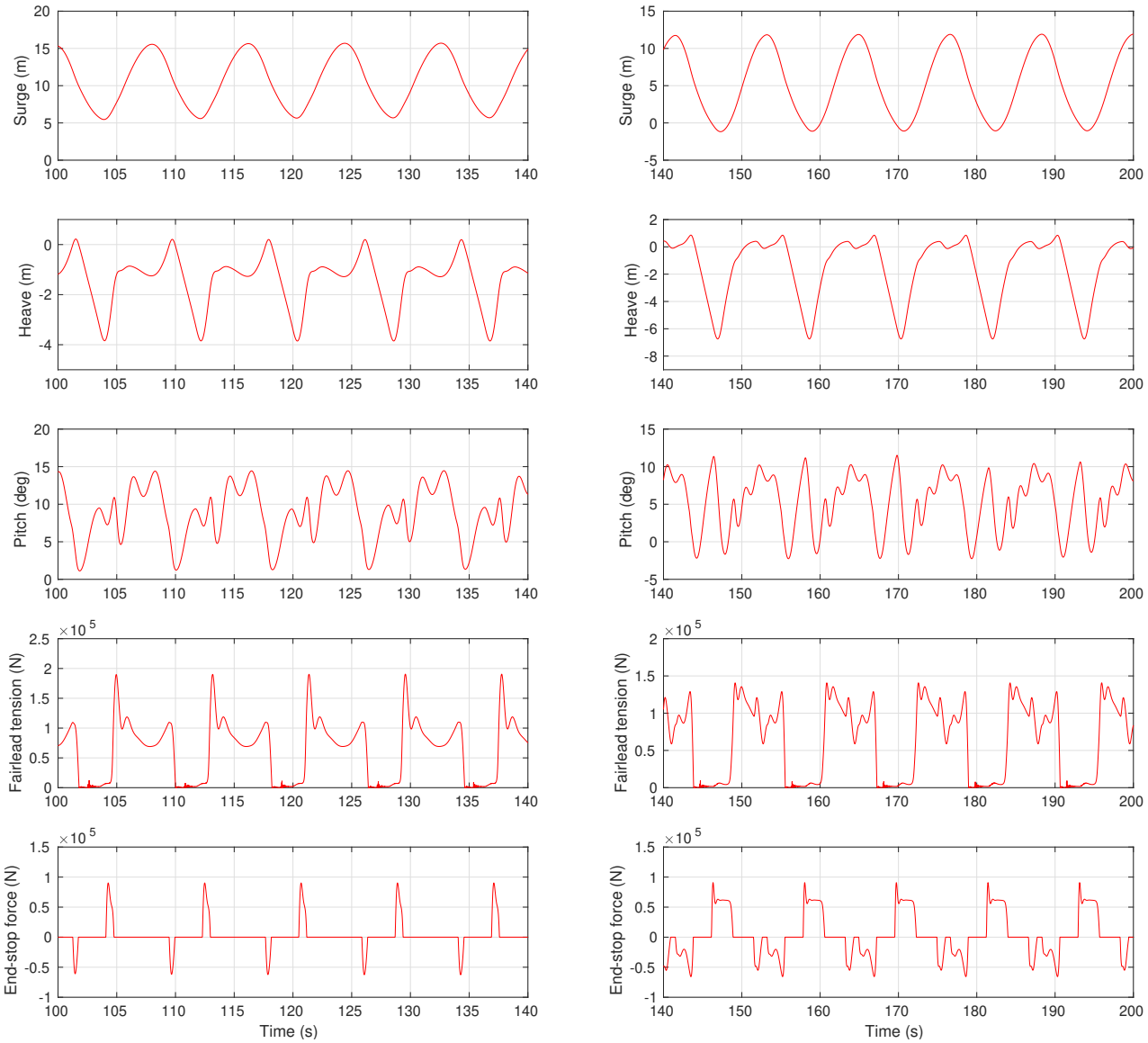

(a) ERW1: $T = 8.2$ s and $H = 9.5$ m.

(b) ERW2: $T = 11.7$ s and $H = 13.3$ m.

Fig. 4. Baseline simulations of the equivalent regular wave ERW1 (left) and ERW2 (right) cases.

The geometry and parameter settings used in this work follow closely the settings of [29] in which extreme loads were investigated using CFD modelling. The wave data is for Humboldt Bay, California. The WEC is located in 70 m water depth and the fluid density is $\rho_w = 1025$ kg/m^3. The generator hull is standing on the bottom, placing the center of the 1.8 m long translator at 67.3 m below the water surface in equilibrium. Table I shows the baseline settings used to simulate the full-scale WEC system.

B. Extreme waves

We follow the work of Katsidoniotaki et al. [29] and investigate two sea states that corresponds to the 100-year contour line. We use two approaches: (i) the equivalent regular wave (ERW) approach [29] and (ii) full 3-hours sea states of irregular waves (IRW) estimated using the JONSWAP spectrum with a spreading factor of $\gamma = 3.3$. The cases are presented in Table II.

Fig. 4 shows the results of the deterministic simulations of the equivalent regular wave cases using the default values (the base case). Most notable is that the positive heave motion is restricted by the limited

TABLE II
WAVE CASES EXAMINED.

Regular waves	H (m)	T (s)
ERW1	9.5	8.2
ERW2	13.3	11.7
Irregular waves	H_s (m)	T_p (s)
IRW1	5.0	8.2
IRW2	7.0	11.7

TABLE III
RANDOM INPUT VARIABLES, DISTRIBUTIONS AND RANGES.

Variable	Distribution	Lower bound	Upper bound
Wave height	Uniform	$0.9H$	$1.1H$
Wave period	Uniform	$0.9T$	$1.1T$
Buoy MoI	Uniform	$0.9I_{yy}$	$1.1I_{yy}$
Buoy CoG	Uniform	$0.9z_b$	$1.1z_b$
Buoy drag	Uniform	$0.5C_D$	$1.5C_D$
Line diameter	Uniform	$0.9D_c$	$1.1D_c$
PTO damping	Uniform	$0.75C_{PTO}$	$1.25C_{PTO}$
End-stop stiffness	Uniform	$0.75K_{es}$	$1.25K_{es}$

strokelength, and the surface buoy is consequently deeply submerged under the wave crest. As the buoy surges back when the wave trough arrives, the mooring goes slack and the translator falls back to hit the lower end-stops. When the mooring goes back in re-tension a snap load is visible.

C. Basic VMEA

From a basic VMEA study we identify eight variables to be investigated in more detail: significant wave height, peak period, mooring line diameter, the moment of inertia of the buoy, the centre of gravity of the buoy, the PTO damping coefficient, the translator friction coefficient, the end-stop spring stiffness and end-stop damping coefficient. They were chosen from having the largest sensitivity coefficients. Please note that the VMEA was performed for the case of the PTO operating as usual. Other cases such as a freely running or stuck generator would potentially have different values. The deterministic or constant parameters of the set-up are presented in Table I. As we are to assess the sensitivity of the variables on the extreme loads, we assume uniform distributions centered around the baseline values (see Table I) with parameter ranges as depicted in Table III.

D. Sensitivity analysis using equivalent regular waves: d=1

We compute solutions on the Experiment of Design (EoD) input points for different orders $P = [4, 5, 6]$ of the gPC (which in this section corresponds to the Smolayk quadrature points). We then construct the gPC surrogate models from these solution samples. This is carried out for the maximum tension at the fairlead and the upper and lower maximum end-stop forces.

Fig. 5 shows some examples of the convergence of the surrogate models for maximum tension of the ERW1 case. The dots show the deterministic solutions at the quadrature points and the solid lines show the resulting gPC surrogate model. We see that for most cases a polynomial order of $P = 4$ is sufficient. Using the surrogate models we perform MC simulations using 1 million samples to obtain the PDFs. The PDFs for the maximum fairlead tension are shown in Fig. 6. Even though the input distribution is uniform, the PDFs are clearly more complicated, which highlights the nonlinearity of the mooring and end-stop system. The resulting statistics are presented in Tables IV and V. It is observed that for the steeper wave case ERW1 the largest variation is associated with the wave parameters, whereas for ERW2 the drag and PTO damping have the largest variation. As the lower end-stop force arise from the translator hitting the end-stop during

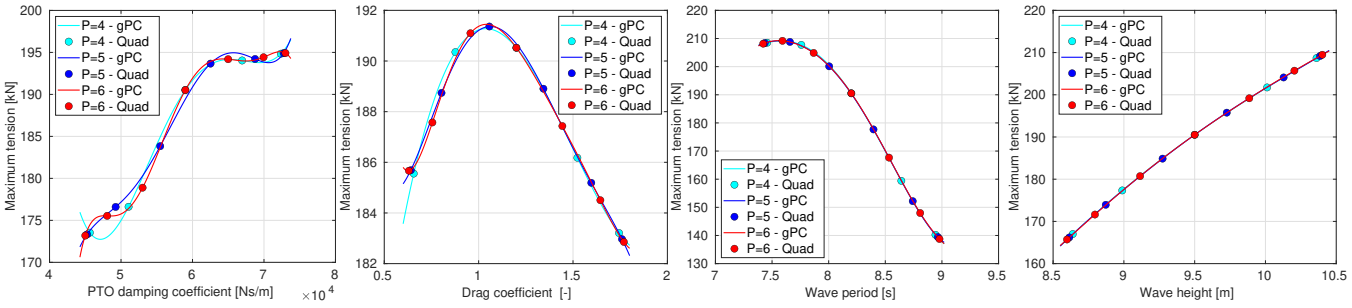

(a) C_{PTO} (b) C_d (c) T (d) H

Fig. 5. Convergence of gPC surrogate models for the maximum tension in the mooring cable at the fairlead. ERW1 case using $d = 1$.

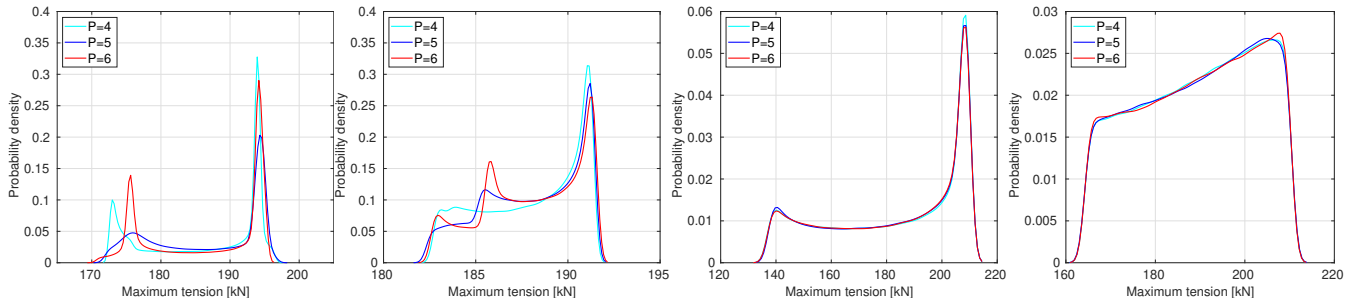

(a) C_{PTO} (b) C_d (c) T (d) H

Fig. 6. Convergence of PDFs for the maximum tension in the mooring cable at the fairlead. ERW1 case using $d = 1$.

TABLE IV
MEAN AND STANDARD DEVIATION OF MAXIMUM FAIRLEAD TENSION, UPPER AND LOWER END-STOP FORCES FOR THE ERW1 CASE USING $d = 1$.

Case	Fairlead tension (kN)		Upper end-stop (kN)		Lower end-stop (kN)	
	Mean	Std dev	Mean	Std dev	Mean	Std dev
H	189.4	13.3	-60.1	4.2	90.2	0.0
T	183.3	24.1	-47.9	25.9	89.9	0.7
I_{yy}	190.5	0.1	-62.7	0.1	90.2	0.0
z_b	189.8	1.3	-62.4	1.5	90.2	0.0
C_d	188.0	2.7	-58.3	16.1	90.0	0.6
D_c	190.4	3.3	-62.5	1.3	90.2	0.2
C_{pto}	186.6	8.2	-45.9	30.3	90.7	11.8
K_{es}	190.4	0.5	-62.4	3.7	90.0	4.9

TABLE V
MEAN AND STANDARD DEVIATION OF MAXIMUM FAIRLEAD TENSION, UPPER AND LOWER END-STOP FORCES FOR THE ERW2 CASE USING $d = 1$.

Case	Fairlead tension (kN)		Upper end-stop (kN)		Lower end-stop (kN)	
	Mean	Std dev	Mean	Std dev	Mean	Std dev
H	139.0	4.7	-66.4	1.2	90.9	0.1
T	140.0	3.8	-65.8	9.5	90.8	0.1
I_{yy}	136.5	0.1	-66.4	0.0	90.9	0.0
z_B	136.3	0.6	-66.6	0.8	90.9	0.1
C_d	142.7	5.9	-64.9	4.6	90.8	0.1
D_c	136.5	0.8	-65.1	2.6	90.9	0.3
C_{pto}	141.4	7.1	-67.4	14.0	92.6	9.8
K_{es}	136.4	0.4	-66.0	2.9	90.8	4.9

TABLE VI
MEAN AND STANDARD DEVIATION OF MAXIMUM FAIRLEAD TENSION, UPPER AND LOWER END-STOP FORCES FOR THE RW1 AND RW2 CASE USING $d = 5$.

Case	Fairlead tension (kN)		Upper end-stop (kN)		Lower end-stop (kN)	
	Mean	Std dev	Mean	Std dev	Mean	Std dev
RW1	183.1	26.5	-46.9	27.3	84.0	23.3
RW2	147.1	9.5	-70.8	15.4	92.2	11.2

TABLE VII
MEAN AND STANDARD DEVIATION OF MAXIMUM FAIRLEAD TENSION, UPPER AND LOWER END-STOP FORCES FOR THE IRW1 AND IRW2 CASES USING $d = 5$.

Case	Fairlead tension (kN)		Upper end-stop (kN)		Lower end-stop (kN)	
	Mean	Std dev	Mean	Std dev	Mean	Std dev
IRW1	278.7	13.9	-187.3	27.7	94.6	11.6
IRW2	269.5	7.5	-222.1	20.2	94.7	11.7

free fall it is only the PTO damping and end-stop stiffness that influence the force.

E. Sensitivity analysis using equivalent regular waves: d=5

To keep the dimension of the problem low, only the five variables with the highest impact (the largest variance) in the $d = 1$ results are identified for further investigation. The investigated variables are: wave height, wave period, drag coefficient, PTO damping and end-stop stiffness. We generate 100 sampling points using the latin hyper cube (LHC), and run the deterministic model with those input variables. The PDFs for the fairlead tension and upper/lower end-stop forces for ERW1 are shown in Fig. 7. The shape of the PDF for the fairlead tension greatly resembles the PDF obtained by $d = 1$ for the wave height, but looking at the sensitivity index in Fig. 8 it is actually the wave period that has the highest sensitivity.

Indeed, for the ERW1 case the $d = 5$ simulation has the same ranking of sensitivity as the $d = 1$ simulations, i.e. in falling order for fairlead tension: H, T, C_{pto}, C_D and K_{es}. For the upper end-stop the ranking is the same between the $d = 1$ and $d = 5$ simulations, but the importance of the PTO damping is enhanced for the $d = 5$ case. Also for the lower end-stop the PTO damping is the most sensitive variable.

Looking at the ERW2 case (Figs. 9 to 10) the PDFs have smaller variances, and sensitivity index differs greatly for the maximum tension in the mooring line. Here the PTO damping dominates whereas wave period and drag have similar importance. The end-stops have similar ranking as for the ERW1 case.

F. Sensitivity analysis using irregular waves: d=5

The equivalent regular wave approach used above is attractive because the simulation times are relatively short. However, it is well-known that the results using ERW differs significantly from full sea-states [30]. Hence, we also investigate the sensitivity using irregular waves by applying the multi-dimensional $d = 5$ analysis. Please note that the random phase angle is not treated within the gPC framework as the resulting dimension would be far too large. Instead we treat the phase angle according to DNVGL-OS-E301 [31], i.e. by running 10 realizations of the sea states for every quadrature point in the LHC (using the same random seeds for the realizations). At every LHC sampling point, the maximum/minimum values found from the 10 realizations are then used in constructing the surrogate models.

The resulting PDFs and Sobol indices are presented in Figs. 11 to 14 and in Table VII. We notice that:

- there are significant differences between the PDFs from the ERW cases and the irregular wave cases. The ERW greatly underestimates the maximum loads in the fairlead and upper end-stop. Only the lower end-stop is similar (for the same reason as before, being governed by the gravity-driven fall of the translator);
- the maximum mooring tension is not associated with the largest waves. This is due to the limited stroke-length of the translator;
- The difference in mean and variance between IRW1 and IRW2 is rather small and within one standard deviation.
- for the mooring tension the most sensitive variable

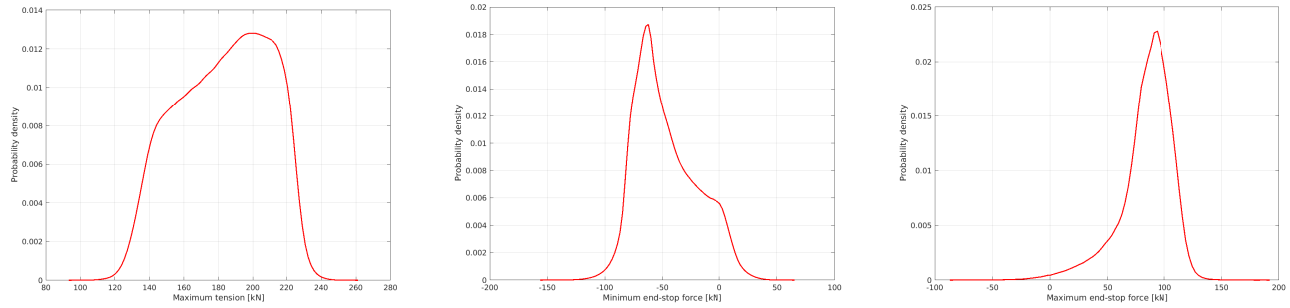

(a) Fairlead tension (b) Upper end-stop force (c) Lower end-stop force

Fig. 7. PDFs for the ERW1 case using $d = 5$.

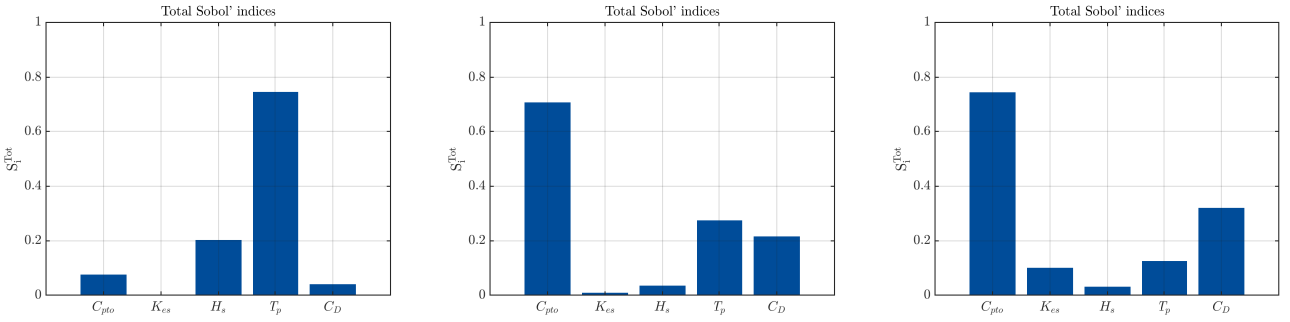

(a) Fairlead tension (b) Upper end-stop force (c) Lower end-stop force

Fig. 8. Total sensitivity index for the ERW1 case using $d = 5$.

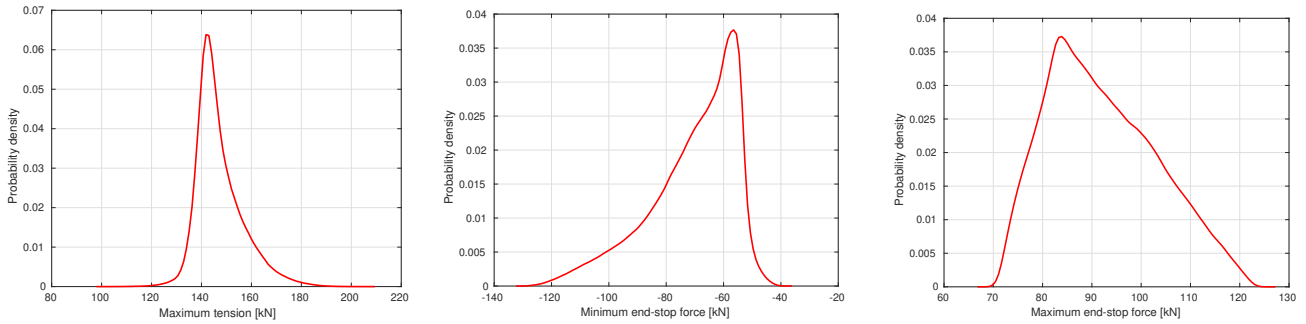

(a) Fairlead tension (b) Upper end-stop force (c) Lower end-stop force

Fig. 9. PDFs for the ERW2 case using $d = 5$.

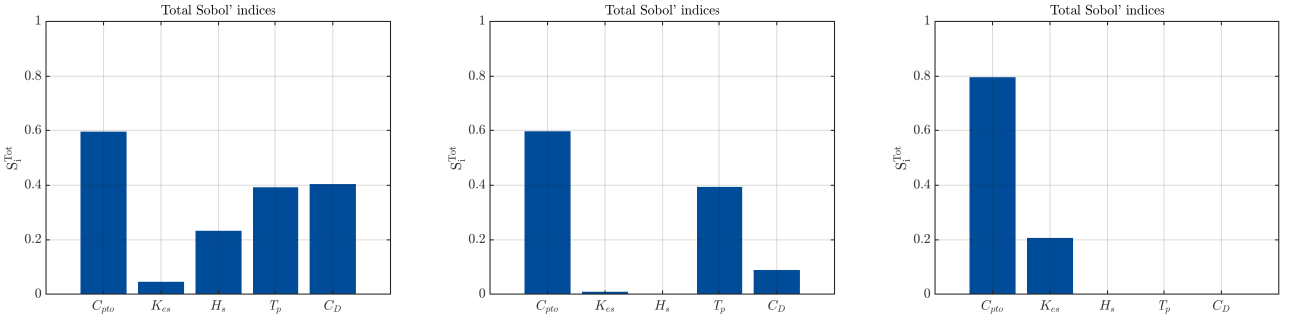

(a) Fairlead tension (b) Upper end-stop force (c) Lower end-stop force

Fig. 10. Total sensitivity index for the ERW2 case using $d = 5$.

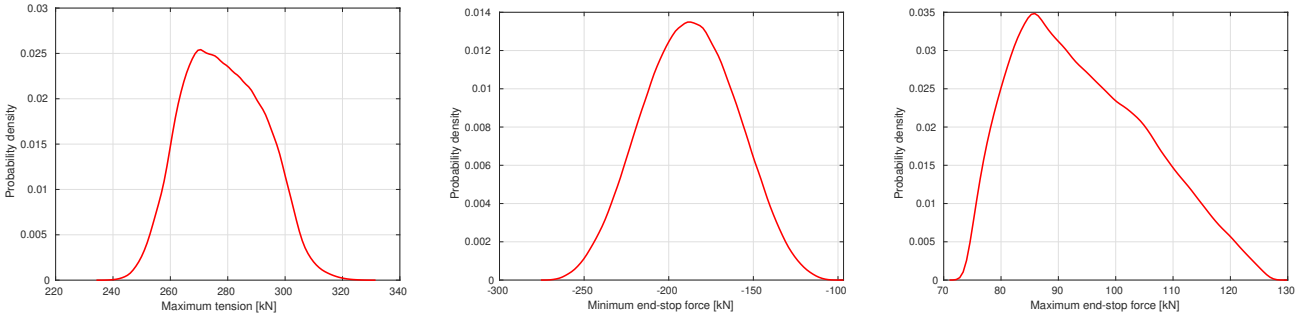

(a) Fairlead tension (b) Upper end-stop force (c) Lower end-stop force

Fig. 11. PDFs for the SS1 case using $d = 5$.

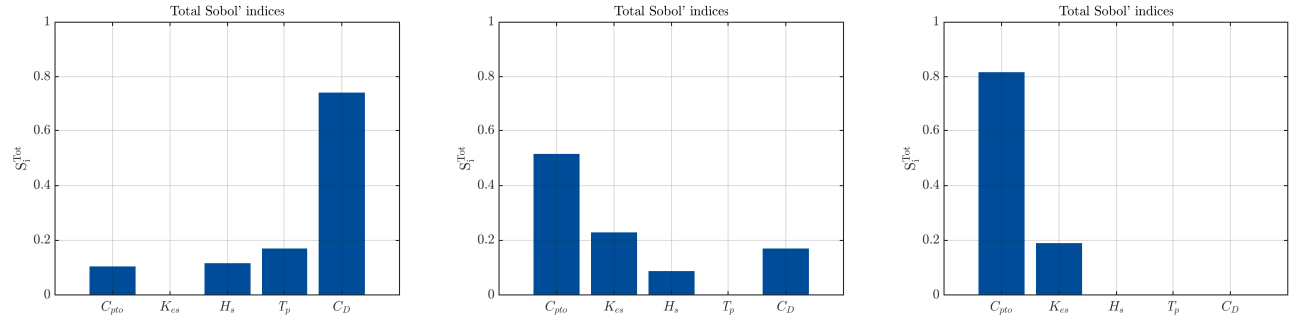

(a) Fairlead tension (b) Upper end-stop force (c) Lower end-stop force

Fig. 12. Total sensitivity index for the SS1 case using $d = 5$.

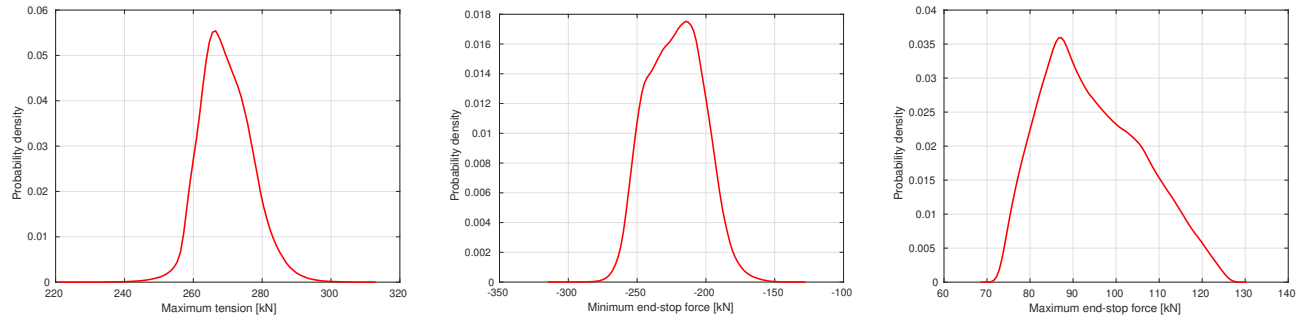

(a) Fairlead tension (b) Upper end-stop force (c) Lower end-stop force

Fig. 13. PDFs for the SS2 case using $d = 5$.

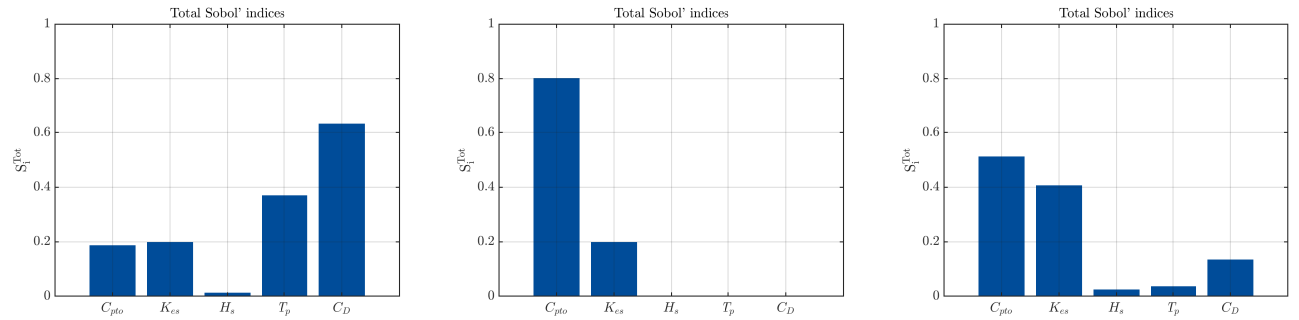

(a) Fairlead tension (b) Upper end-stop force (c) Lower end-stop force

Fig. 14. Total sensitivity index for the SS2 case using $d = 5$.

is the buoy drag coefficient, which has a larger impact in the irregular waves than in the ERW cases.

VI. Concluding remarks

We have performed a sensitivity analysis of extreme loads for mooring and end-stop forces for a taut-moored point-absorber (the Uppsala Universty WEC). From a basic VMEA we identified eight input variables associated with the largest uncertainties, covering: the design case (significant wave height and peak period), the surface buoy (centre of gravity, moment of inertia, drag coefficient), the PTO (PTO damping, end-stop stiffness) and the mooring line (line diameter).

Surrogate models based on gPC were created for regular waves; both single dimension cases (one variable at a time, $d = 1$) and multi-dimensional ($d = 5$) cases. We also illustrated that a rather low polynomial order ($p = 4$) could be used. Surrogate modelling yields great savings compared to MC simulations using the full deterministic model. To simplify the analysis of the irregular wave cases, the random phase angles wave components were not treated in the gPC approach. However, we still needed a fair amount of simulations to construct the surrogate models. For the cases presented we used 10 phase seeds and 100 LHC samples giving 1000 simulations per sea state. Large differences were seen between using equivalent regular waves and irregular waves, both in terms of mean, variance and sensitivity indices. Thus, it is recommended to use full sea-states for the case of extreme loads on the UU WEC.

Finally, it should be mentioned that the significant over-topping of the WEC that takes place raises some concerns about the numerical accuracy of the linear potential flow simulations for these load cases. This problem can be addressed by constructing the surrogate models in a multi-fidelity manner combining linear potential flow and CFD simulations.

References

[1] Clean Technica. (2010). [Online]. Available: https://cleantechnica.com/2010/05/22/massive-offshore-waves-sink-australias-oceanlinx-wavepower-pilot/

[2] Renew Economy. (2014). [Online]. Available: https://reneweconomy.com.au/ceto-wave-energy-machine-destroyed-cyclone-reports-say/

[3] Ny Teknik. (2017). [Online]. Available: https://www.nyteknik.se/energi/jag-tror-inte-att-seabased-fullfoljer-projektet-6830164

[4] SMHI. (2017). [Online]. Available: https://www.smhi.se/data/oceanografi/havsvagor/rekord-vaghojd-1.9314

[5] R. Coe, Y.-H. Yu, and J. van Rij, "A survey of WEC reliability, survival and design practices," *Energies*, vol. 11, p. 4, 2018.

[6] Y. Zhao and S. Dong, "Probabilistic fatigue surrogate model of bimodal tension process for a semi-submersible platform," *Ocean Engineering*, vol. 202, p. 108501, 2021.

[7] C. Li, J. Choung, and M.-H. Noh, "Wide-banded fatigue damage evaluation of catenary mooring lines using various artificial neural networks models," *Marine Structures*, vol. 60, pp. 186–200, 2018.

[8] D. Xiu and G. E. Karniadakis, "The Wiener-Askey polynomial chaos for stochastic differential equations," *SIAM Journal on Scientific Computing*, vol. 24, no. 2, pp. 619–644, jan 2002.

[9] D. Xiu, *Numerical Methods for Stochastic Computations - A Spectral Method Approach*. Princeton, New Jersey: Princeton University Press, 2010.

[10] D. Bigoni, A. Engisg-Karup, and C. Eskilsson, "Efficient uncertainty quantification of a fully nonlinear and dispersive water wave model with random inputs," *Journal of Engineering Mathematics*, vol. 101, pp. 87–113, 2016.

[11] G. M. Paredes, J. B. Thomsen, F. Ferri, and C. Eskilsson, "Mooring system reliability analysis of an ORE device using general Polynomial Chaos," in *Proc. of the 13th European Wave and Tidal Energy Conference*, no. 1271, Naples, Italy, September 1-6 2019.

[12] G. Paredes, C. Eskilsson, and A. Engsig-Karup, "Uncertainty quantification of mooring cable dynamics using polynomial chaos expansions," *Journal for Marine Science and Engineering*, vol. 8, p. 162, 2020.

[13] P. T. T. Nguyen, L. Manuel, and R. G. Coe, "On the development of an efficient surrogate model for predicting long-term extreme loads on a wave energy converter," *Journal of Offshore Mechanics and Arctic Engineering*, vol. 141, no. 6, p. 061103, 2019.

[14] A. Chakhunashvili, P. Johansson, and B. Bergman, "Variation Mode and Effect Analysis," in *Proc. of the Annual Reliability and Maintainability Symposium*, 2004, pp. 364–369.

[15] P. Johannesson, T. Svensson, L. Samuelsson, B. Bergman, and J. de Mare, "Variation Mode and Effect Analysis: an application to fatigue life prediction," *Quality and Reliability Engineering International*, vol. 25, pp. 167–179, 2009.

[16] M. Leijon, O. D. C. Boström, S. Gustafsson, K. Haikonen, O. Langhamer, E. Strömstedt, M. Stålberg, J. Sundberg, O. Svensson, S. Tyrberg, and R. Waters, "Wave energy from the North Sea: Experiences from the Lysekil research site," *Surveys in Geophysic*, vol. 29, no. 3, pp. 221–240, 2008.

[17] National Renewable Energy Laboratory and Sandia Corporation, "WEC-Sim (Wave Energy Converter SIMulator) — WEC-Sim documentation," 2021. [Online]. Available: https://wec-sim.github.io/WEC-Sim/

[18] J. Palm and C. Eskilsson, *MOODY, User's manual version 1.0*, 2018, avaliable www.github.com/johannep/moodyAPI/releases.

[19] P. Johannesson, T. Svensson, and H. Gaviglio, "Reliability evaluation using Variation Mode and Effect Analysis: Application to Corpower's mooring pre-tension cylinder," in *Proceedings of the 13th European Wave and Tidal Energy Conference (EWTEC)*, Napoli, Italy, September 2019.

[20] I. Sobol, "Sensitivity estimates for nonlinear mathematical models," *Mathematical and Computer Modelling*, vol. 1, pp. 407–414, 1993.

[21] S. Marelli, C. Lamas, K. Konakli, C. Mylonas, P. Wiederkehr, and B. Sudret, "UQLab user manual - Sensitivity analysis," Chair of Risk, Safety & Uncertainty Quantification, ETH Zurich, Zurich, Tech. Rep. UQLab-V1.2-106, 2019.

[22] W. Cummins, "The impulse response function and ship motions," *Schiffstechnik*, vol. 9, pp. 101–109, 1962.

[23] A. Babarit and G. Delhommeau, "Theoretical and numerical aspects of the open source BEM solver NEMOH," in *11th European Wave and Tidal Energy Conference* , ser. Proceedings of the 11th European Wave and Tidal Energy Conference, Nantes, France, 2015.

[24] J. Palm, C. Eskilsson, and L. Bergdahl, "An hp-adaptive discontinuous Galerkin method for modelling snap loads in mooring cables," *Ocean Engineering*, vol. 144, pp. 266–276, 2017.

[25] J. Palm and C. Eskilsson, "Influence of bending stiffness on snap loads in marine cables: A study using a high-order discontinuous galerkin method," *Journal of Marine Science and Engineering*, vol. 8, no. 10, 2020. [Online]. Available: https://www.mdpi.com/2077-1312/8/10/795

[26] ——, "Mooring systems with submerged buoys: influence of buoy geometry and modelling fidelity," *Applied Ocean Research*, vol. 102, p. 102302, 2020. [Online]. Available: http://www.sciencedirect.com/science/article/pii/S0141118719307709

[27] ——, "On end-stops and snap loads for taut moored wave energy converters," in *Proc. 14th European Wave and Tidal Energy Conference*, Plymouth, U.K., 2021.

[28] G. M. Paredes, C. Eskilsson, J. Palm, J. P. Kofoed, and L. Bergdahl, "Coupled BEM/*hp*-FEM modelling of moored floaters," in *Proceedings of the 1st Vietnam Symposium on Advances in Offshore Engineering*. Hanoi, Vietnam: Springer, November 2018, pp. 504–510.

[29] E. Katsidoniotaki, E. Ransley, S. Brown, J. Palm, J. Engström, and M. Göteman, "Loads on a point-absorber wave energy converter in regular and focused extreme wave events," in *Proc. of the ASME 2020 39th International Conference on Ocean, Offshore and Arctic Engineering*, no. OMAE2020-18639, Fort Lauderdale, FL, USA, June 28-July 3 2020.

[30] M. Hann, D. Greaves, and A. Raby, "Snatch loading of a single taut moored floating wave energy converter due to focussed wave groups," *Ocean Engineering*, vol. 96, pp. 258–271, 2015.

[31] *Position Mooring*, Det Norske Veritas, 2010, offshore standard DNV-OS-301.